5.3

STATISTICAL PATTERNS IN AEROSOL RETRIEVALS FROM NOAA/AVHRR AND TRMM/VIRS

Alexander Ignatov*, Istvan Laszlo, Nicholas Nalli
Climate Research and Applications Division, NOAA/NESDIS/ORA, Camp Springs MD 20746

1. INTRODUCTION

Aerosol retrievals are made operationally at NESDIS from the Advanced Very High Resolution Radiometer (AVHRR) onboard the afternoon NOAA satellites (Rao et al. 1989, Stowe et al. 1997) and experimentally at NASA/Langley Research Center (LaRC) from the Visible and InfraRed Scanner (VIRS) onboard the Tropical Rainfall Measuring Mission (TRMM) satellite (Ignatov and Stowe 2000). The two radiometers are nearly identical in their scanning geometry, and the relative simplicity of their measurement scheme. Both instruments have only two spectral channels (out of five), useful for aerosol studies, centered at λ_1=0.63, λ_2=0.83 μm for AVHRR, and λ_1=0.63, λ_2=1.61 μm for VIRS. The parameters being retrieved are aerosol optical depths, AOD, in the two channels, τ_1 and τ_2, and Angstrom exponent, AE, $\alpha=-\ln(\tau_1/\tau_2)/\ln(\lambda_1/\lambda_2)$. This paper compares three τ_1-products: two from AVHRR, and one from VIRS.

2. NOAA/AVHRR VS. TRMM/VIRS

NOAA orbits are circular (altitude H~870 km) polar (inclination I~98.8E) sun-synchronous (period T~102 min). They are designed to over-fly underlying surface around T_o~1:40 LT, but the actual overpass time slightly varies around T_o (with a full repeat cycle of ~9 days), and it drifts towards later afternoon during satellite lifetime. AVHRR scans cross-track within ~"67E of nadir (sub-satellite swath ~2,600 km), thus providing daily near-global coverage with a nadir field of view (FOV) resolution ~4 km (Global Area Coverage; GAC). Aerosol retrievals have been made since June 1981 (NOAA-7) over global oceans (~70ES-70EN).

TRMM was launched in November 1997 into a circular (H~350 km) tropical (I~35E) non-sun-synchronous orbit (T~91 min), providing coverage from 40ES-40EN. This orbital configuration results in a varying local observation time from orbit to orbit, eventually spanning the full diurnal range during the TRMM repeat cycle of ~46 days. VIRS scans cross-track within ~"48E of nadir (FOV~2 km at nadir), which corresponds to a sub-satellite swath of ~720 km. TRMM leaves gaps between orbits, and takes longer times to provide global coverage compared to NOAA.

* *Corresponding author address*: Alexander Ignatov, E/RA1, Rm.712, WWBG, NOAA, 5200 Auth Rd., Camp Springs, MD 20746-4304. e-mail: Alex.Ignatov@noaa.gov

3. AEROSOL RETRIEVALS

An aerosol retrieval algorithm is applied to cloud-glint-free calibrated satellite sensor data. Both data quality and algorithm are important for accurate retrievals.

3.1 Data Pre-Processing

Accurate cloud screening to the satellite data is difficult, and it is critical for aerosol retrievals. The transition from aerosol to cloud is blurred, and even a small amount of unscreened (e.g. sub-pixel) cloud may dramatically affect aerosol retrievals. Cloud screening in the three products is accurate yet different (Stowe et al. 1999; Trepte et al. 1999; Ignatov and Nalli 2002).

Only data with Sun zenith 2_o<60° are used. Current algorithms make retrievals away from sun glint area (γ>40°). Historically, data on the solar side of orbit are excluded, too (Stowe et al. 1997).

Radiometric factors may cause significant errors in aerosol retrievals (Ignatov 2002). The AVHRR and VIRS are calibrated following Rao and Chen (1999); Nguyen et al. (2002). VIRS channel 2, strongly contaminated by thermal leak, is of limited use for aerosol retrievals.

3.2 Single-Channel Algorithm

Aerosol retrievals from AVHRR and VIRS are highly under-determined. In the NESDIS algorithm, aerosol phase function was derived empirically (Ignatov 1997), and later fit with Mie calculations for a mono-modal log-normal size distribution (dN/dlogR) with R_m=0.1 μm, σ= 2.03, n=1.4-0*i*. This model is prescribed and non-variable. Recent improvements to the algorithm documented in Ignatov and Stowe (2002a) are associated with the use of a more versatile and accurate 6S radiative transfer model (Vermote et al. 1997).

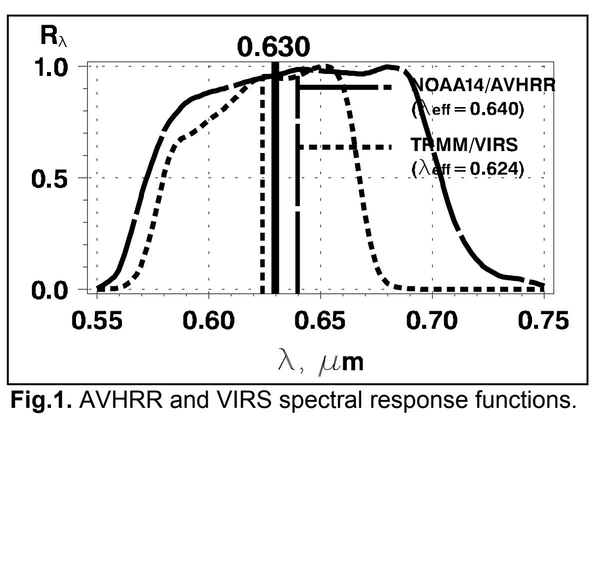

Fig.1. AVHRR and VIRS spectral response functions.

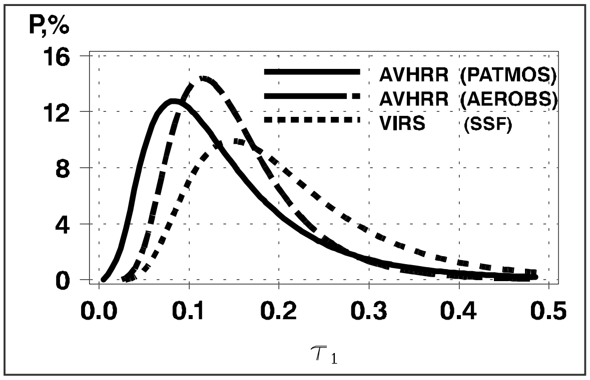

Fig.2. Log-normal fit to the empirical τ_1-histograms ($\Delta\tau$= 0.02). Fit parameters (for definitions of geometric mean and STD, see O'Neill et al. 2000): τ_g=0.126, μ=1.81 (PATMOS); τ_g=0.140, μ=1.55 (AEROBS); τ_g=0.183; μ=1.64 (VIRS). Corresponding arithmetic statistics (customarily used in literature): τ_m=0.149, σ=0.094 (PATMOS, N=87,166); τ_m=0.154, σ=0.083 (AEROBS, N=355,607); τ_m=0.207; σ=0.115 (VIRS, N=605,214).

Retrievals are made taking into account the sensor-specific spectral filters (Fig.1), and scaled over to a monochromatic wavelength of 0.63 μm, representative of all AVHRR sensors onboard different NOAA satellites, and VIRS (Ignatov and Stowe 2002a).

Surface reflectance has two components: Lambertian (ρ=0.002 at 0.63 μm) and bi-directional (Cox-Munk; wind speed 1 m s^{-1}). Rayleigh scattering and gaseous absorption are calculated for the mid-latitude summer atmospheric model.

3.3 AVHRR/VIRS Data Used in This Study

Global AVHRR (operational AEROBS product, ~8-km resolution; N=355,607) and VIRS (Single Satellite Footprint, SSF (Edition 2B) with a variable resolution, ~10-km at nadir; N=605,214, cross-track only) data were collected from 2-10 April 1998. The choice of a 9-day period is historically due to the NOAA 9-day repeat cycle, and may not be fully representative for TRMM with its 46-day repeat cycle. Due to different spatial and temporal resolution/sampling, their pixel-by-pixel merge is not straightforward. The comparison is therefore done statistically. We also use a second AVHRR dataset here, Pathfinder Atmosphere (PATMOS, ~110-km resolution; N=87,166) merged with buoy matchups. Representative of 8 years of data collected from two satellites (NOAA11, 1991-94; and NOAA14, 1995-98), it is useful to provide a "climatological" perspective to the shorter AEROBS and VIRS datasets.

3.4 Potential Use of AVHRR/VIRS Second Channel

The second channel on AVHRR/VIRS can be used for estimating the aerosol model simultaneously with τ, and for the derivation of a second aerosol parameter, the Angstrom Exponent, α (Ignatov et al. 1998; Higurashi and Nakajima 1999; Mishchenko et al. 1999). The accuracy of α, and improvements to τ depend upon errors in the individual channels, and their amplification through the spectral separation (Ignatov et al. 1998). It is intuitively expected that the potential of AVHRR for aerosol retrievals is limited. AVHRR channels are not calibrated onboard, they are spectrally wide and strongly contaminated by gaseous absorption, and not separated enough in spectrum. Ignatov and Stowe (2002b) attempted to formalize these intuitions by using a concept of information content. They found that the signal-to-noise ratio in α is well approximated as η~τ/τ_o. This formula is generally true for all satellite data, and different satellite products differ by the value of τ_o only. Below τ_o, errors in satellite retrievals of α exceed natural variability in the Angstrom exponent, and are useless, and they become progressively more meaningful as τ increases beyond τ_o. For AEROBS, τ_o~0.18 (Ignatov and Stowe 2002b); for PATMOS, τ_o~0.11 (Ignatov and Nalli 2002). These τ values are fairly typical over oceans, which indicates that the accuracy of α, derived from AVHRR channels 1 and 2, and resulting improvements to τ, are marginal under typical open ocean conditions. For VIRS, τ_o has not yet been estimated, due to the thermal leak in its 1.61 μm channel. AVHRR τ_1-data have been quality controlled as described in Ignatov and Stowe (2002b; AEROBS) and Ignatov and Nalli (2002; PATMOS). The SSF VIRS Edition 2B data are used "as is." This study uses only the first channel of both sensors.

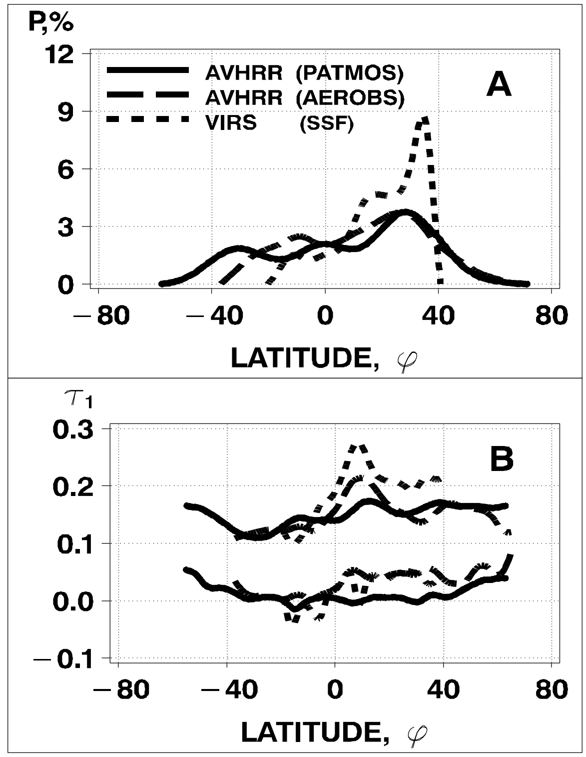

Fig.3. Latitude a) frequency distribution; and b) zonal trends in the mean τ_m and minimum, τ_{min} ($\Delta\varphi$=2°). (Note that in Figs.3-6, τ_m is calculated arithmetically).

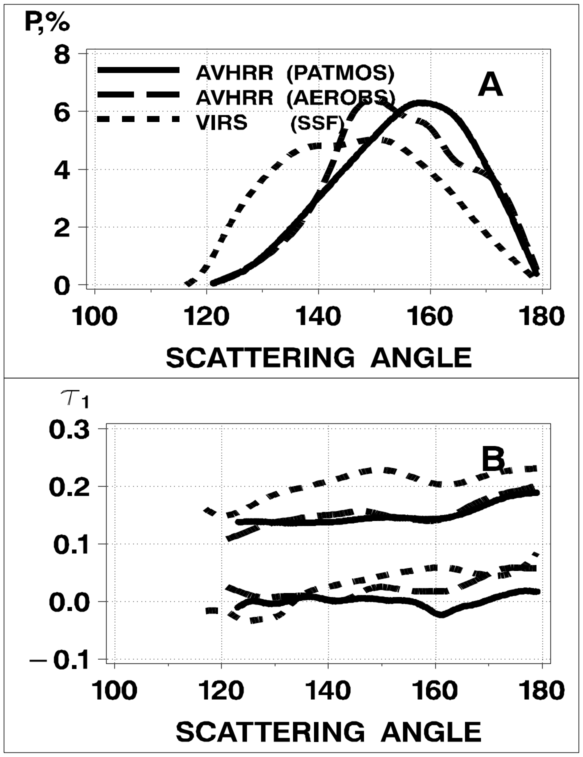

Fig.4. Scatter angle: (a) frequency distribution, and (b) trends in the mean, τ_m, and minimum, τ_{min} ($\Delta\chi$=2°).

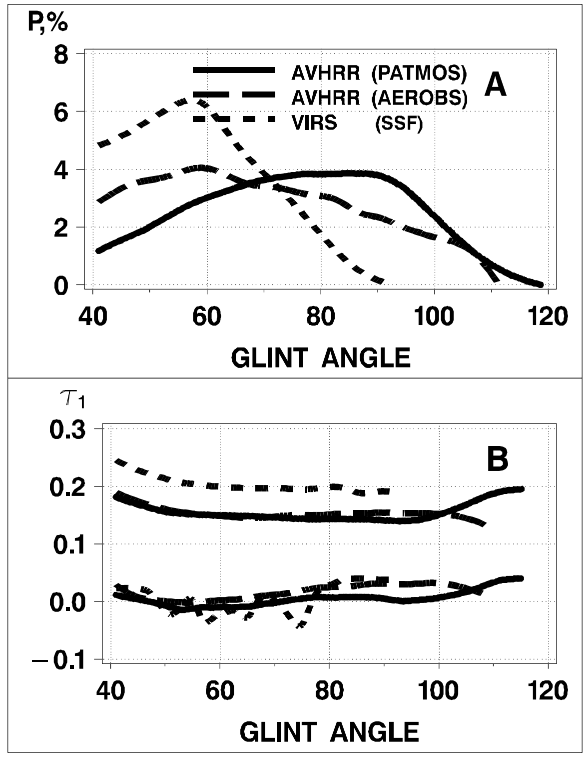

Fig.5. Glint angle: (a) frequency distribution, and (b) trends in the mean, τ_m, and minimum, τ_{min} ($\Delta\gamma$=2°).

4. RESULTS

Fig.2 plots histograms of τ_1. All of them are close to a log-normal shape (O'Neill et al. 2000; Ignatov and Stowe 2002b). The high bias in AEROBS with respect to PATMOS suggests a positive anomaly of $\delta\tau_1$~+0.014 in April 1998 compared to the AVHRR 8-year average. The 9-day AEROBS and VIRS data agree well at low τ_1, but begin to diverge as τ_1 increases. The differences between AEROBS and VIRS are significant, and may be due to differences in sampling (covering different domains in space/time or scattering/reflection geometry), cloud screening, and/or calibration.

Fig.3a plots the zonal distribution of retrievals. VIRS data are distributed from 20°S-40°N, with ~80% of points found in the Northern Hemisphere. AVHRR data are distributed more uniformly between the two Hemispheres. Note that AEROBS is lacking data below 40°S, due to the seasonal pattern of AVHRR coverage.

Fig.3b plots respective zonal trends in τ_m and τ_{min}. AEROBS positive anomaly with respect to PATMOS 8-year climatology is clearly traced from 0°-20°N in τ_m, and from 0°-40°N in τ_{min}. VIRS retrievals show this anomaly exaggerated.

Another observation from Fig.3 is that the VIRS τ_{min} traces closely its AEROBS counterpart (except a few dropouts in VIRS τ_{min}, which result from the lack of AVHRR-like quality control applied to the VIRS data Ignatov and Stowe 2002a), which makes the hypothesis of their calibration-induced differences less plausible. According to the analyses by Ignatov (2002), calibration error affects not only τ_m but τ_{min} as well, albeit to a somewhat lesser extent.

Figs.4-5 examine the effect of possible differences in the scattering (χ) and reflection (γ) geometry. For the 9-day period, VIRS retrievals tend to be taken at lower χ and γ angles than AVHRR. On average, τ_m is angle-independent, with two exceptions: τ_m shows increasing trend at χ>160°, and at γ<50°. These may suggest the need for adjustments to the phase function, and to the bi-directional surface reflectance, used in the retrievals.

Retrievals of τ_1 from AVHRR and VIRS are made from radiances, averaged over all cloud-free pixels within a certain spatial domain, and the cloudy portion of that domain is used to estimate the cloud amount, A. Fig.6 plots histograms of A, and respective trends in τ_1, from PATMOS (estimated with statistically equivalent spatial coherence technique, SESC, Stowe et al. 1999) and SSF data (Trepte et al. 1999). [Note: 1) the cloud amount plotted is a conditional estimate: Only those cells which have at least one pixel suitable for aerosol retrieval were used; 2) A is not available from AEROBS]. The histograms of A are shaped differently: The SSF peaks at A~0% and declines monotonically at A>0, whereas PATMOS peaks at A~50%. Average cloud amount is A_m~9% (σ_A~16%) in SSF, and A_m~38% (σ_A~19%) in PATMOS. The A_m-difference is much larger than one could expect from different spatial scales in PATMOS and SSF. Despite large differences in A,

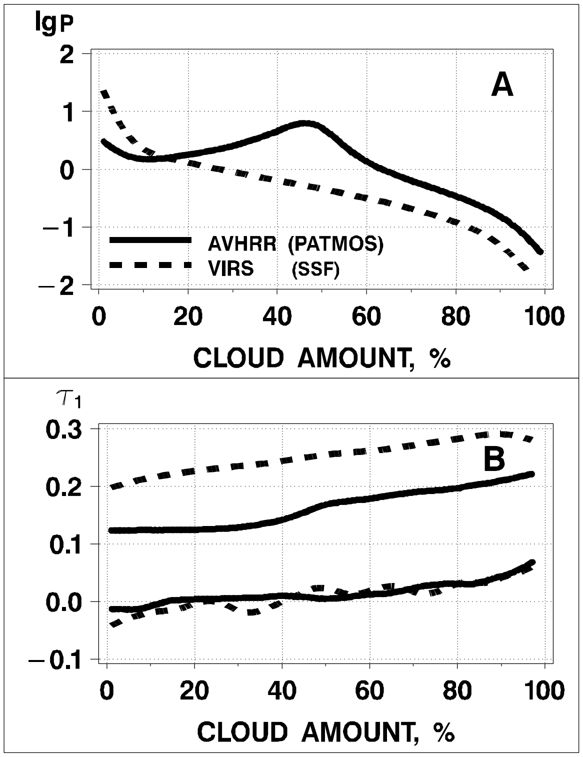

Fig.6. Cloud amount: (a) frequency distribution (note that $\log_{10}P$ is plotted), and (b) trends in the mean, τ_m, and minimum, τ_{min} (ΔA=2%).

dependence of τ_1 on A is very significant and similar in SSF and PATMOS.

5. CONCLUSION

Aerosol optical depths, τ_1, have been derived from AVHRR and VIRS at 0.63 μm using a single-channel algorithm. Improvements to τ_1, resulting from the use of second channel, have been analyzed elsewhere and found marginal for typical τ_1 used in this study.

Preliminary analyses suggest that τ_1 reveal similar statistical patterns. In particular, the shape of probability density functions is close to log-normal. Zonal and angular τ_1-trends track each other closely. VIRS τ_1 are biased high with respect to AVHRR. Different sampling (spatial and scattering/reflection geometry) and calibration seem to be unlikely causes for the observed τ_1-differences. The largest differences are observed in the cloud amount patterns, suggesting that the different cloud screening in the two datasets may be the primary cause.

Acknowledgement. Contributions from L.Stowe, N.Rao, B.Wielicki, W.Miller, and E.Geier were critical. Thanks go to J.Sapper, P.Minnis, T.Charlock, J.Coakley, N.Loeb, D.Young, S.Kato, F.Rose, R.Arduini, W.Su, W.Collins, C.Moeller for helpful advice. The TRMM SSF data were obtained from the Atmospheric Sciences Data Center at the NASA/LaRC. L.Hunt, K.Morris, L.Mathias are acknowledged for the help with data access. A.Ignatov and N.Nalli are CIRA visiting scientists at NESDIS. This study was supported by the EOS/CERES Project (NASA contract L-90987C), and by the Ocean Remote Sensing Program at NOAA/NESDIS.

References

Higurashi A., T.Nakajima, 1999: Development of a Two-Channel Aerosol Retrieval Algorithm on a Global Scale Using NOAA/AVHRR. *JAS,* **56**, 924-941.

Ignatov A., 1997: Estimating aerosol phase function in backscatter from AVHRR and sun-photometer measurements. *JAM*, **36**, *6*, 688-694.

Ignatov A., 2002: Sensitivity and information content of aerosol retrievals from AVHRR: Radiometric factors. *Appl.Opt.*, **46**, *6*, 991-1011.

Ignatov A., and N.Nalli, 2002: Aerosol Retrievals from Multi- Year Multi-Satellite AVHRR Pathfinder Atmosphere (PATMOS) Dataset for Correcting Remotely Sensed Sea Surface Temperatures. *JTECH*, in press.

Ignatov A., and L.Stowe, 2000: Physical basis, premises, and self-consistency checks of aerosol retrievals from TRMM/VIRS. *JAM*, **39**, *12*, 2259-2277.

Ignatov A., and L.Stowe, 2002a: Aerosol retrievals from individual AVHRR channels: I. Retrieval algorithm and transition from Dave to 6S radiative transfer model. *JAS*, **59**, *3(1)*, 313-334.

Ignatov A., and L.Stowe, 2002b: Aerosol retrievals from individual AVHRR channels: II. Quality control, probabi-lity distribution functions, information content, and consistency checks of retrievals. *JAS*, **59**, *3(1)*, 335-362.

Ignatov A., et al., 1998: Sensitivity study of the Ångström exponent derived from AVHRR over oceans. *Adv. Space Res.,* **21**, *3*, 439-442.

Nguyen, et al., 2002: Rapid calibration of operational and research meteorological satellites: III. Calibration of sun-synchronous satellites. *JTECH*, in press.

O'Neill N., et al., 2000: The log-normal distribution as a reference for reporting aerosol optical depth statistics: empirical tests using multi-year, multi-site AERONET sun-photometer data. *GRL*, **27**, *20*, 3333-3336.

Rao N., and J.Chen, 1999: Revised post-launch calibration of the visible and near-IR channels NOAA14/AVHRR. *IJRS*, **20**, 3485-3491.

Stowe L., et al, 1997: Development, validation, and potential enhancements the second generation operational aerosol product at NOAA/NESDIS. *JGR*, **102**, *D14*, 16923-16934.

Stowe L., et al., 1999: Scientific basis and Initial Evaluation of the CLAVR-1 Global Clear/Cloud Classification Algorithm for AVHRR. *JTECH*, **16**, 656-681.

Trepte Q., et al., 1999: Scene identification for the CERES cloud analysis subsystem. Proc. AMS 10th Conf. Atmos. Rad., Madison, WI, Jun 28-Jul 2, 169-172.